Functional and phylogenetic evidence of a bacterial origin for the first enzyme in sphingolipid biosynthesis in a phylum of eukaryotic protozoan parasites

John G. Mina[1], Julie K. Thye[2], Amjed Q.I. Alqaisi[1,3], Louise E. Bird[4], Robert H. Dods[2], Morten K. Groftehauge[2], Jackie A. Mosely[2], Steven Pratt[1], Hosam Shams-Eldin[5], Ralph T. Schwarz[5], Emhke Pohl[1,2], Paul W. Denny[1*]

From the [1]Department of Biosciences, Durham University, Lower Mountjoy, Stockton Road, Durham, DH1 3LE; [2]Department of Chemistry, Durham University, Lower Mountjoy, Stockton Road, Durham, DH1 3LE; [3]Biology Department, College of Science, University of Baghdad, Baghdad, Iraq; [4]Oxford Protein Production Facility UK, Research Complex at Harwell, Rutherford Appleton Laboratory, Didcot, OX11 0FA, UK; [5]Institut für Virologie, Zentrum für Hygiene und Infektionsbiologie, Philipps-Universität Marburg, Hans-Meerwein-Strasse, 35043 Marburg, Deutschland

Running title: *The apicomplexan serine palmitoyltransferase*

To whom correspondence should be addressed: Paul W. Denny, Department of Biosciences, Durham University, Lower Mountjoy, Stockton Road, Durham, DH1 3LE, U.K. Telephone: +44 (0)191 3343983; Email: p.w.denny@durham.ac.uk

Key words: *Toxoplasma gondii,* parasite metabolism, evolution, serine palmitoyltransferase, sphingolipid, Apicomplexa, small angle X-ray scattering

ABSTRACT

Toxoplasma gondii is an obligate, intracellular eukaryotic apicomplexan protozoan parasite that can cause fetal damage and abortion in both animals and humans. Sphingolipids are essential and ubiquitous components of eukaryotic membranes that are both synthesized and scavenged by the Apicomplexa. Here we report the identification, isolation and analyses of the *Toxoplasma* serine palmitoyltransferase, an enzyme catalyzing the first and rate-limiting step in sphingolipid biosynthesis - the condensation of serine and palmitoyl-CoA. In all eukaryotes analyzed to date, serine palmitoyltransferase is a highly conserved heterodimeric enzyme complex. However, biochemical and structural analyses demonstrated the apicomplexan orthologue to be a functional, homodimeric serine palmitoyltransferase localized to the endoplasmic reticulum. Furthermore, phylogenetic studies indicated that it was evolutionarily related to the prokaryotic serine palmitoyltransferase, identified in the Sphingomonadaceae as a soluble homodimeric enzyme. Therefore this enzyme, conserved throughout the Apicomplexa, is likely to have been obtained via lateral gene transfer from a prokaryote.

Toxoplasma gondii is an obligate, intracellular protozoan parasite, which is able to invade and colonize a wide variety of nucleated vertebrate cells. It is a member of the Apicomplexa, a diverse phylum including important pathogens of humans and domestic animals such as *Plasmodium* (the causative agent of malaria), *Cryptosporidium* (diarrhoea)*, Eimeria* (coccidiosis in poultry) and *Theileria* (East Coast Fever in Cattle). *Toxoplasma* has emerged as an important opportunistic pathogen and toxoplasmosis is one of the primary opportunistic diseases in the immunocompromised, particularly AIDS patients, those receiving anti-cancer chemotherapy and organ transplant recipients (*1*). *Toxoplasma* infection *in utero* is also a significant cause of spontaneous abortion in economically important domestic animals (*2*) and congenital defects in humans (*1*) .

As an intracellular parasite, *Toxoplasma* has a dynamic relationship with its host cell, including both the synthesis and scavenging of key lipid species (3,4), such as sphingolipids (*5-*

7). Sphingolipids are amphipathic lipids consisting of a sphingoid backbone acylated with a long-chain fatty acid and having a polar head group. Whilst the basic sphingolipid, ceramide, is a secondary signalling molecule involved in, for example, apoptosis (*8-10*), modified or complex sphingolipids are major components of the outer leaflet of eukaryotic plasma membranes involved, together with sterols, in the formation of micro-domains commonly known as lipid rafts. These domains have been proposed to function in a diverse array of processes from the polarised trafficking of lipid-modified proteins, to the assembly and activation of signal transduction complexes (*11*). The first, rate-limiting enzyme in sphingolipid biosynthesis is serine palmitoyltransferase (SPT), a pyridoxal phosphate (PLP)-dependent class II aminotransferase which catalyses the Claisen-like condensation of L-serine and, typically, palmitoyl-CoA to form 3-ketodihydrosphingosine (KDS) (*12*) (Figure 1). Subsequently, *N*-acylation of the sphingoid base in the endoplasmic reticulum (ER) leads to the formation of ceramide. Following transport to the Golgi apparatus, ceramide is used to form modified or complex sphingolipids, sphingomyelin (SM) or glycosphingolipid (GSL) for example (10,13). In all eukaryotes studied to date SPT is composed of a core heterodimer of two evolutionary related proteins that spans the membrane of the ER (*14*). One subunit, LCB2, contains the canonical PLP-binding and catalysis domain, whilst the other (LCB1) is not thought to bind this co-factor but to be important for complex stability (*12*). Both subunits are essential for enzyme activity in *Saccharomyces cerevisiae* (*15*), and analyses of temperature sensitive SPT mutants have demonstrated that *de novo* synthesis of sphingolipids and their precursors is pivotal in a wide spectrum of cellular processes including endocytosis, stress responses and protein trafficking (*16-18*). Members of the Prokaryota also encode a functional SPT, which was first characterised in *Sphingomonas paucimobilis* (12,19). However in contrast to the eukaryotic paralogue, the bacterial enzyme is a soluble, homodimeric PLP-dependent class II aminotransferase and has been proposed to represent an evolutionary precursor of the heterodimeric eukaryotic SPT (*20*). Despite the divergence in primary sequence, the crystal

structure of the *S. paucimobilis* enzyme revealed a symmetrical dimer with the co-factor PLP bound to each subunit in a manner predicted to be conserved in the eukaryotic SPT subunit, LCB2 (*21*).

Like other eukaryotes apicomplexan *Toxoplasma* and *Plasmodium* spp. synthesize sphingolipids *de novo*, including both SM and GSLs (5,22,23). Sphingolipid-enriched lipid micro-domains have been implicated in the interaction of *Plasmodium falciparum* with the host erythrocyte (*24*). However, host sphingolipid biosynthesis is non-essential for the proliferation of *Toxoplasma* (6,7), indicating that *de novo* synthesis is important for parasitism (*3*). *Toxoplasma* were known to produce both SM and GSLs (*5*), but until recently the mechanics of sphingolipid metabolism in *Toxoplasma,* and other apicomplexans, remained enigmatic. However, the first functionally characterised enzyme in the apicomplexan sphingolipid biosynthetic pathway has now been described as an orthologue of the yeast inositol phosphorylceramide (IPC) synthase (an enzyme with no mammalian equivalent) (*6*). To enable further understanding and analyses, the identification and characterisation of the key enzyme components in the apicomplexan *de novo* pathway is essential. Whilst our characterisation of the *Toxoplasma* IPC synthase has initiated this process (*6*) significant gaps remain, not least the formal identification of the apicomplexan SPT, the first and rate limiting step in sphingolipid biosynthesis (*12*). Importantly, in the absence of a defined SPT, the incorporation of tritiated serine into sphingolipid species during metabolic labelling of isolated *Toxoplasma* and *P. falciparum* indicated the presence of an active apicompexan SPT (22,25).

Here we describe the identification and characterisation of the *Toxoplasma* SPT, which represents a new class of eukaryotic enzyme with a very surprising, prokaryotic, origin. These studies shed new light on the evolution of these protozoan parasites, and present a paradigm shift in the way the origin of sphingolipid biosynthesis is considered.

RESULTS

A putative apicomplexan serine palmitoyltransferase-In all eukaryotes studied to date, including members of the protozoa, the first enzyme in the sphingolipid biosynthetic pathway, SPT (*13*), is composed of 2 related subunits (LCB1 and LCB2) (*26*). However, initial BLAST searches of the complete, annotated genome databases of both *Toxoplasma gondii* and *Plasmodium falciparum* (http://toxodb.org; http://plasmodb.org), using a range of LCB1 and LCB2 protein sequences, failed to locate genes encoding either SPT subunit. Given that both of these parasites have been shown to possess SPT activity (22,25) this represented a major paradox. Further interrogation of the *Toxoplasma* genome database using BLAST and the conserved 10 residue PLP-binding domain (PROSITE consensus PS00599) common to all eukaryotic SPT LCB2 proteins (*27*), identified two closely related (68% identical), tandemly encoded, predicted type II PLP-dependent aminotransferases with no known function. Surprisingly, the putative PLP-binding sites from both proteins were both completely conserved with respect to the 12 residue PLP-binding motif (GTFSKSXXXXGG) identified in the Sphingomonadaceae bacterial SPT (*28*). Further analyses demonstrated that the best characterised bacterial SPT, from *Sphingomonas paucibmobilis,* showed limited homology with the identified *Toxoplasma* proteins: 28 and 30% identity, and 47 and 46% similarity, in the C-terminal region (64% of total predicted protein) of TgSPT1 and 2 respectively (*20*). In addition, using the BLAST tool and the predicted *Toxoplasma* protein sequences, singly encoded orthologues of the putative apicomplexan SPT were also found in the genome databases of *Plasmodium* spp. and the chicken pathogen, *Eimeria tenella*. Comparison of the primary amino acid sequences of the putative apicomplexan proteins with the bacterial SPT indicated the presence of an *N*-terminal extension, which harbours a transmembrane region absent in the prokaryotic polypeptide (Figure 2).

Taken together, these observations clearly indicated that the putative apicomplexan SPT is radically different to those of all other eukaryotes studied thus far. To prove this, it was vital to demonstrate the functionality of the apicomplexan SPT.

TgSPT1 is a functional serine palmitoyltransferase-The complete open reading frame of the predominant, tachyzoite expressed, *Toxoplasma* SPT, TgSPT1 (see toxodb.org, transcriptomic data), was cloned into the yeast expression vector, pRS426-MET, to create pRS426-TgSPT1. In the auxotrophic yeast strain YPH499-HIS-GAL-LCB2 the essential PLP-binding, catalytic SPT subunit LCB2 (*15*) is under the control of a GAL1 promoter. In non-permissive glucose-containing SD medium, which inhibits expression from the GAL1 promoter, the yeast are non-viable. Transformation with pRS426-TgSPT1 allowed the growth of YPH499-HIS-GAL-LCB2 in this media, as did the ectopic expression of *S. cerevisiae* LCB2. In contrast, the empty vector, pRS426-MET, did not rescue the growth of the auxotrophic yeast strain (Figure 3). These data strongly indicate that TgSPT1 is a functional orthologue of the *S. cerevisiae* LCB2 and, therefore, at least part of the *T. gondii* serine palmitoyltransferase.

To analyse the functionality of TgSPT1 *in vitro* a series of constructs were made in collaboration with the Oxford Protein Purification Facility (OPPF-UK) in the vector pOPINS3C, where the insert is *N*-terminally fused to a cleavable *N*-HIS SUMO tag (29,30). Following triage based on expression levels and product solubility, a series of these fusion proteins (with *N*-terminal deletions of 143, 158, 176 and 180 amino acids) were expressed, purified and subjected to preliminary functional analyses using palmitoyl-CoA and ^{14}C-labelled serine as substrates (Supplemental 1). The truncated construct TgSPT1 Δ158 was selected for further analyses. Mass spectrometry demonstrated the reaction product of the enzyme to be KDS (Figure 4), and therefore TgSPT1 is a *bona fide* SPT.

To further understand enzyme function small-angle X-ray scattering (SAXS) was utilized to determine the shape of the protein in solution and investigate whether TgSPT1 forms a homodimer similar to the bacterial orthologue. The results are summarized in Figure 5A which shows the experimentally derived shape of the molecule in grey as a bead model, and superimposed a ribbon diagram of the homodimeric homology model of *Tg*SPT1 based on the known crystal structure of the *S. paucimobilis* SPT (*21*). The *ab initio* envelope

3

shows very good agreement with the homo-dimeric model, where the core of the enzyme adopts a similar conformation to the bacterial orthologue. The elongated shape of the envelope indicated increased conformational flexibility of the termini of the protein. Using the homology model of the TgSPT1 dimer, the theoretical X-ray scattering data calculated with CRYSOL (*31*) revealed some discrepancies with the experimental data (Figure 5B). Whilst the shape of the curve was similar, the low intensity values are higher in the experimental data consistent with a more elongated/or larger shape as shown in the *ab initio* envelope. Furthermore, the homology model indicated that the co-factor PLP can bind precisely to the predicted binding motifs in each monomer at the dimer interface of the structural model (Figure 5C). Therefore, the *Toxoplasma,* and by extension the apicomplexan, SPTs are functional as homodimers. This resembles the bacterial situation (*19*) rather than the so far universal eukaryotic model of core heterodimeric modality (*14*). However, in contrast to the Prokaryota where SPT is a soluble enzyme (*20*), the eukaryotic enzyme complex is associated with the membrane of the endoplasmic reticulum (*14*). As discussed above the *N*-terminal extension contains a predicted transmembrane domain and the data indicate that this does not influence functionality *in vitro*. It is noteworthy that Uniprot (www.uniprot.org) has predicted the *P. falciparum* SPT *N*-terminal region to target the protein to the apicoplast (*32*), a vestigial plastid that harbours the machinery for several lipid biosynthetic pathways (*33*). However, the ability of TgSPT1 to complement for a deficiency of LCB2 in auxotrophic mutant yeast (Figure 3) indicated that the protozoal enzyme is targeted to the ER, which is the locale for SPT activity in this and other eukaryotes (*14*). Episomal expression of tagged TgSPT1-TY and the ER marker GFP-HDEL (34,35) allowed co-localisation by immuno-fluorescence microscopy, and indicated that TgSPT1 is an ER rather than apicoplast localised enzyme in *Toxoplasma* (Figure 6A-D). Furthermore, using a rat polyclonal antibody raised against TgSPT1 Δ158, the native protein was shown to have a similar ER localization pattern (Figure 6E-H). Looking at a larger vacuole showed the same localization pattern of native TgSPT1 (Figure 7A-D). In addition, the larger

quantity of data available here facilitated quantitative co-localisation analyses illustrated by scatterplots (Figure 7E-G). These show 2-dimensional histograms of differentially labelled cell compartments (see axes labels for the channel/wavelength) at the same spatial region. A linear correlation demonstrates a strong spatial correlation between the channels, the slope indicates the relative intensities (36,37). The plot in Figure 7E demonstrated a strong correlation of TgSPT1 (antiSPT-AF594) with GFP-HDEL (antiGFP-AF488) and ER localisation. In contrast, neither TgSPT1 (antiSPT-AF594) nor GFP-HDEL (antiGFP-AF488) showed any significant correlation with DAPI-stained nuclei (Figure 7F and G). In an additional control experiment TgSPT1 (antiSPT-AF594) showed no significant correlation with episomally expressed, cytosolic GFP (Supplemental 2). Together, these data demonstrated that TgSPT1 has a canonical eukaryotic subcellular localisation, the ER.

In summary, TgSPT1 represents a new class of eukaryotic SPTs found in the Apicomplexa. Whilst it functionally and structurally resembles the prokaryotic enzymes its membrane localisation, and place in an apparently conventional eukaryotic synthetic pathway (*6*), demonstrate it serves a conventional eukaryotic role.

A surprising evolutionary origin for the apicomplexan serine palmitoyltransferase-The data presented above detail the identification and functional characterisation of TgSPT1, a eukaryotic enzyme, which in terms of its primary sequence and homodimeric structure, resembles the prokaryotic 'sister' enzymes.

Our comprehensive sequence searches of the protozoan genome databases identified closely related orthologues of TgSPT1/2 in *Plasmodium* spp., *Eimeria tenella* and *Cryptosporidium muris*. Unlike *Toxoplasma* these members of the Apicomplexa maintain a single SPT copy, indicating that TgSPT1 and 2 resulted from a gene duplication event that occurred post-speciation of the phylum. Interestingly, *C. hominis* and *C. parvum*, unlike *C. muris*, completely lack any gene encoding for SPT, despite the genomic region being syntenic between all three species (Figure 8A). This suggests that *C. hominis* and *C. parvum* have selectively lost the first and rate-limiting step in sphingolipid biosynthesis,

4

probably reflecting a specific adaptation of the parasite-host relationship.

To further analyse the evolutionary origin of the divergent apicomplexan SPT, phylogenetic analyses of a conserved region, including the PLP binding-site, were carried out. Using CLUSTALW (38) to align the predominant conserved region (Figure 2; Supplemental 3), followed by Fitch Margoliash Distance (F-MDist) (39); Randomized Axelerated Maximum Likelihood (RAxML) (40) and Phylogeny Maximum Likelihood (PhyML) (41) the relationship of the apicomplexan SPT with both the eukaryotic catalytic subunit, LCB2, and the prokaryotic homodimeric SPT were determined (Figure 8B). It was clear that the apicomplexan sequences do not represent conventional eukaryotic LCB2, with the kingdom to which they belong, the Chromalveolatea, split across the two major clades. The predicted catalytic subunits of the SPT from the Chromalveolate *Thalassoira pseudonana* and *Phytophthora ramorum* group with high certainty with the conventional LCB2 subunits, however the apicomplexan SPTs form a clade, supported by bootstrap values, with the prokaryotic sequences. This bioinformatic approach strongly indicated that the homodimeric apicomplexan enzyme is a divergent eukaryotic SPT of prokaryotic origin.

DISCUSSION

The *Toxoplasma* serine palmitoyltransferase, TgSPT, was identified as being encoded by two closely related genes, and was found to be conserved as a single copy throughout the Apicomplexa. TgSPT1 demonstrated the ability to complement an auxotrophic yeast LCB2 mutant and functionality was confirmed by analyses of expressed and purified TgSPT1. However, the predicted protozoan enzyme is highly divergent compared with the heterodimeric enzyme characterized throughout the Eukaryota. Small angle X-ray scattering (SAXS), coupled with homology modelling, demonstrated that the protein forms a homodimer, thereby resembling the prokaryotic rather that the eukaryotic paralog. This relationship was further confirmed by phylogenetic analyses which demonstrated the apicomplexan sequences as being most closely related to the prokaryotic SPT, with the protozoan SPT showing divergence from the catalytic SPT

subunit (LCB2) in all other eukaryotes, including fellow members of the Chromalveolata. These data strongly indicated that the apicomplexan SPT was derived from horizontal transfer from a prokaryotic species (probably a member of Alphaproteobacteria) and demonstrated the evolution of eukaryotic sphingolipid biosynthesis is more complex than previously recognised. These data also add to the evolutionary complexity of the Apicomplexa, protozoan parasites known to harbour a vestigial plastid (the apicoplast) as a remnant of an ancient algal endosymbiotic event (42).

EXPERIMENTAL PROCEDURES

Bioinformatics analyses- The 10 residue canonical, degenerate, PLP-binding domain common to all eukaryotic SPT subunit 2 proteins (43) was used to search the complete genome database of *Toxoplasma gondii* (toxodb.org) with WU-BLAST (Gish, W. (1996-2003) http://blast.wustl.edu). 2 hits were identified - TGME49_090980 (TgSPT1) and TGME49_090970 (TgSPT2). The protein sequence of TgSPT1 and WU-BLAST were subsequently used to search the *Plasmodium, Eimeria* and *Cryptosporidium* genome databases (plasmodb.org and genedb.org). NCBI-BLAST was used to compare the hits against the NCBI protein sequence database. Exploiting the structural data available for the bacterial *S. paucimobilis* enzyme (*21*), representatives of the apicomplexan and bacterial SPTs were aligned using T-Coffee Expresso (44). The resulting multiple sequence alignment was reformatted in T-Coffee with the command "t_coffee -other_pg seq_reformat -in <msa> -output sim" to yield the identity values.

TgSPT1 isolation and cloning-Toxoplasma gondii RH *hxgprt-* were propagated in vero cells (both kind gifts from Dominique Soldati-Favre, University of Geneva, Switzerland) and isolated as described previously (45). RNA was then extracted using the RNeasy® kit (Qiagen) according to the yeast protocol. Following quantitation using Nanodrop® 2000 (ThermoFisher) cDNA was synthesized using random primers and the SuperScript® III kit (ThermoFisher) as directed by the manufacturer. Full length TgSPT1 was then amplified by PCR using the proof-reading DNA polymerase *Pfu*

5

(Promega) and primers TgSPT5'HindIII CCC**AAGCTT**GC<u>ATG</u>GCTTCGGGTGCAACG TACTTC and TgSPT3'NotI ATAAGAAT**GCGGCCGC**<u>TCA</u>TCGGAGCAT GTCAGTGGGTGGG (restriction sites in bold). The coding sequence was then cloned into the pET24a vector (Novagen). Subsequently, a series of deletion constructs were cloned into a series of pOPIN bacterial expression and, following transformation in a variety of *Escherichia coli* strains, screened for expression of soluble protein at the Oxford Protein Production Facility (OPPF) using their standardized protocols for high throughput analyses (*30*).

Yeast complementation-The YPH499-HIS-GAL- LCB2 *S. cerevisiae* strain was constructed in YPH499 (Mat a; ura3-52; lys2-801amber; ade2-101ochre; trp1-63; his3-200; leu2-1) (Stratagene) by bringing the expression of the yeast LCB2 gene under the control of the stringently regulated GAL1 promoter that is repressed in the presence of glucose as described before (25,46). The following primer sequences were used for amplification of the HIS/GAL cassette: (a) sequence for integration upstream of the coding region (nucleotides -200 to -150) Lcb2HisGalS,

TAAGTTTCATTACTATTTTCTATTATTATCT GCAACTTTTTATTAGTTAGgggcgaattggagctcc ac; (b) sequence for integration at the initiation codon (nucleotides +1 to +50 Lcb2HisGalAS, TAAGTTTCATTACTATTTTCTATTATTATCT GCAACTTTTTATTAGT TAGgggcgaattggagctccac. The numbers indicate the nucleotide positions in the *S. cerevisiae* DNA sequence, with the adenosine of the ATG initiation codon being defined as position +1. The 19 bp sequences at the 3′ ends of these oligonucleotides that are homologous to the sequences of the vector pGAL/HIS3 and serve as a template for amplification of the GAL1/HIS3-cassette are shown in lower case. Transformation into the haploid YPH499 strain, selection on minimal medium lacking histidine but containing galactose and confirmation of the insertion of the HIS–GAL fragment were performed as previously (46). YPH499–HIS–GAL–LCB2 was maintained in SGR medium (4% galactose, 2% raffinose, 0.17% Bacto yeast nitrogen base, 0.5% ammonium sulphate) with galactose/raffinose rather than non-permissive dextrose as the carbohydrate source. For rapid cultivation of the mutant, YPGR medium (4% galactose, 2% raffinose, 1% yeast extract, 2% peptone) was routinely used.

The *S. cerevisiae* lcb2 coding region was amplified from genomic DNA (Invitrogen) using primers (Sclcb2SEcoRI GGG**GAATTC**ATGAGTACTCCTGCAAACTA TACCCG and Sclcb2ASXhoI GGG**CTCGAG**AACAAAATACTTGTCGTCCT TACAATC, restriction sites shown in bold) and the product cloned into pRS426MET25 to create pRS426 ScLCB2. Similarly, the TgSPT1 coding sequence was amplified (TgSPT5′SpeI **ACTAGT**<u>ATG</u>GCTTCGGGTGCAACGTACTT C and TgSPT3′HindIII CGC**AAGCTT**<u>TCA</u>TCGGAGCATGTCAGTGG GTGG, restriction sites in bold) and cloned into the yeast expression vector to create pRS246 TgSPT1. The YPH499–HIS–GAL–LCB2 *S. cerevisiae* strain was transformed with pRS426 ScLCB2 or pRS426 TgSPT1 and functionally complemented transformants selected on non-permissive SD medium (0.17% Bacto yeast nitrogen base, 0.5% ammonium sulfate and 2% dextrose) containing the nutritional supplements necessary to allow selection of transformants.

TgSPT1 protein production and purification-At OPPF four *N*-terminal deletion constructs (TgSPT1 Δ143, Δ158, Δ177 and Δ180) in the pOPINS3C vector (containing a HIS-SUMO-tag and a 3C protease cleavage site) showed good expression levels of soluble protein in Rosetta II (DE3) pLysS *E. coli* grown in Overnight Express™ Instant TB Auto-induction Media (Novagen) with 50 µg/mL ampicillin, 35 µg/mL chloramphenicol (Sigma Aldrich). Protein production was scaled up to 2 L baffled flasks using the same media and conditions, incubated at 37°C until OD_{600} reached 0.5 then the temperature was reduced to 25°C (TgSPT1 Δ158, Δ177 and Δ180) and incubation continued for a further 24 hours, or 15°C (TgSPT1 Δ143) and 48 hours. Following harvesting of the cells by centrifugation and freeze-thawing at -80°C, the pellets were suspended in lysis buffer (50 mM Tris, pH 7.5, 500 mM NaCl, 20 mM imidazole, 0.2 % Tween 20® (v/v), 10 µg/ml DNAse, 10 µg/ml RNAse [all Sigma Aldrich], and EDTA-free protease inhibitors [Roche]) before lysis by

sonication and isolation of the soluble fraction following centrifugation. HIS-SUMO-tagged TgSPT1 fusions were then isolated using a His trap FF 5 ml column (GE Healthcare Life Sciences) equilibrated with 50 mM Tris, pH 7.6, 500 mM NaCl, 20 mM imidazole, 25 µM pyridoxal-5-phosphate (PLP) and 5 % glycerol (v/v) (all Sigma Aldrich), and FPLC (Akta). Bound protein was then eluted in 50 mM Tris, pH 7.6, 500 mM NaCl, 1 M imidazole, 25 µM pyridoxal-5-phosphate (PLP) and 5 % glycerol (v/v) before dialysis into 10 mM Tris, pH 7.6, 150 mM NaCl, 25 µM pyridoxal-5-phosphate (PLP) and 5 % glycerol (v/v) using Slide-A-Lyzer cassette (Thermo Scientific). To cleave the purification tag, the dialysis step was performed in the presence of the Human RhinoVirus 3C Protease (HRV 3C; Qiagen). Following concentration using a spin concentrator (Agilent Technologies) samples were injected onto on a 1 ml MonoQ 5/50 GL anion exchange column (GE Healthcare) pre-equilibrated with wash buffer (10 mM Tris, pH 8, 100 mM NaCl) using FPLC. The flow-through, containing cleaved and purified protein, was collected, concentrated and dialysed in appropriate buffers, and quantified using a Nanodrop® 2000.

TgSPT enzymatic assay-Initially, TgSPT1 activity was assessed using a methodology based on a published radio-chemical assay (*21*). In a 500 µl reaction volume (50 µM HEPES, pH 7.6, 150 mM KCl, 0.2 mM EDTA, 5 % glycerol, 25 µM PLP), 20 µM of the purified protein was reacted with 20mM L-[^{14}C]-serine (GE Healthcare) and 1.6 mM palmitoyl CoA (Sigma Aldrich) for 75 minutes at 37°C. The organic phase was isolated following the addition of 1 ml CHCl$_3$:CH$_3$OH 2:1 v/v and analyzed by high-performance thin layer chromatography (Merck) in a CHCl$_3$:CH$_3$OH:NH$_4$OH, 40:10:1, solvent system. Images were captured using a AR-2000 Radio-TLC and Imaging Scanner (Bioscan). Subsequently, mass spectrometry was utilized to definitively identify the reaction products under the same conditions as above, but using cold serine and 5-fold greater volumes. Following purification as above, reaction products were analysed, and accurate masses obtained, using a Thermo-Finnigan LTQ FT Mass Spectrometer.

Subcellular localization of TgSPT1- Primers were designed to amplify the *Tg*SPT1 coding sequence: TgSPT5′EcoRV CGC**GATATC**ATGGCTTCGG GTGCAACGTACTTC and TgSPT3′NsiI CGC**ATGCAT**TCGGAGCATGTCAGTGGGTG G, restriction sites in bold. The resultant PCR product was cloned into pTUB8MycGFPPfMyoAtailTy-HX (kind gift from Dominique Soldati-Favre) (47) to create pG1-TgSPT1-TY. Transfections were carried out using a 4D Nucleofector (Lonza), protocol #FI 158 and 20µl reaction volumes in 16 reaction strips. Briefly, *Toxoplasma* were maintained in human foreskin fibroblasts (HFF, ATCC). Parasites freshly lysed from one T75 flask of HFF cells were homogenised by passage through a G25 needle and isolated by centrifugation at 1500g for 10 minutes at 4°C. The pellet was re-suspended in the P3 buffer with added supplement (Lonza) and *Toxoplasma* concentration adjusted to 10^7ml^{-1}. 20µl of this parasite suspension was added to a dried pellet of ethanol-precipitated ~10µg P30-GFP-HDEL (kind gift from Kristin Hager, University of Notre Dame, USA) (48), and/or pG1-TgSPT1-TY plasmid transferred to the transfection strips and electroporated. Subsequently, 100µl media was added and 10µl or 20µl were added to 24-well plates containing confluent HFF cells grown on glass cover slips. The plates were incubated at 37°C, 5.0% CO$_2$ for the appropriate time period.

Cells were fixed in 4% paraformaldehyde (PFA) in phosphate buffered saline (PBS; pH 7.4) for 15 minutes, then permeablised with 0.4% (v/v) Triton X-100 in PBS for 10 minutes, before incubation in blocking buffer (PBS supplemented with 1% (w/v) bovine serum albumin (BSA; Sigma Aldrich), 0.1% Fish Skin Gelatin (Sigma Aldrich) and 0.1% (v/v) Triton X-100) for 15 minutes at room temperature. Samples were incubated with a mouse monoclonal anti-TY antibody (1:200; kind gift from Keith Gull, University of Oxford, UK) or the primary anti-TgSPT1 Δ158 rat polyclonal (Cambridge Research Biochemicals, 1:200), and an anti-GFP rabbit polyclonal antibody (Clontech, 1:200) in blocking buffer overnight at 4°C. After PBS washing, samples were incubated with Alexa Fluor® 594 anti-rat and Alexa Fluor® 488 anti-rabbit secondary antibodies (ThermoFisher) at 1:500 in blocking buffer for 1 hour at room

7

temperature. Samples were incubated with 4',6-diamidino-2-phenylindole (DAPI; Sigma Aldrich) in PBS for 10 minutes, mounted using Vectashield H-1000 (Vector labs) and sealed with nail polish before imaging.

All images were obtained using laser scanning confocal microscope Zeiss LSM 880 with AiryScan equipped with excitation laser 405, Argon 458, 488, 514, He Ne 543, 594 & 633 and AiryScan Filter Set Combinations BP 420-480 + BP 495-550, BP 420-480 + BP 495-620, BP 420-480 + LP 605, BP 465-505 + LP 525, BP 495-550 + LP 570 and BP 570-620 + LP 645. For each image, the dynamic range was checked to avoid saturation, except with the DAPI stain where host cells masked the detection of parasite nuclei at low gain/laser power values. AiryScan images were automatically processed using default values. Zeiss CZI images were exported to TIFF file format using Zen (Blue Edition v2.3, Carl Zeiss Microscopy GmbH, 2011) and analysed using ImageJ Fiji package (49). Co-localisation was assessed using the ScatterJn plugin and scatter plots (36,37). The scatterplots show 2-dimensional histograms of two channels at the same spatial region. Data points are generated as $n(x,y)$, n = number of pixels in each channel and x,y = discrete values 0-255, and displayed as a scatterplot of 256×256 matrix in which the element (x,y) contains the number of data points with coordinates (x,y). The number of pixels is represented by a colour scale. A linear correlation demonstrates a strong spatial correlation between the channels, the slope indicates the relative intensities. Negative controls were checked between DAPI and the Golgi marker, pTub-GRASP-RFP (50), and no positive correlation was found.

Homology modeling-The TgSPT1 homology model was constructed using the Δ158 SPT sequence with the HHPred server (http://toolkit.tuebingen.mg.de/hhpred (51)), which identified the crystal structure of SPT from *S. multivorum* (52) as the closest orthologue (pdb code 3A2B) and aligned the sequences based on sequence identity and the predicted secondary structure of TgSPT1 and the actual secondary structure of 3A2B. The biologically relevant homodimer was used as a template to produce 5 preliminary models with MODELLER (53). The model with the lowest *molpdf* score was taken forward to the next step where PLP was added based on the known bacterial SPT structure. After another minimizing step, the two loops of residues 472-494 that are absent in the bacterial structure were modeled using MODELLER (54). The optimal conformation was based on the lowest *molpdf* and *DOPE* scores, as well as manual inspection using interactive computer graphics.

Small Angle X-ray Scattering-SAXS data was collected using the Δ158 SPT construct on beamline B21 at the Diamond Light Source in size exclusion chromatography HPLC mode (55). Prior to data collection the sample was concentrated to approximately 5 mg/ml. The elution peak was exposed for 5 minutes. Images collected after the 4th minute mark showed signs of radiation damage by analysis of radius of gyration, and were discarded. The raw images were processed and the background subtracted in DAWN (56) at the beamline. Low q values outside the linear part of the Guinier plot were removed in ScÅtter along with q > 0.2519 and Dmax calculated to 133 Å. Further data processing was performed using ATSAS (57). PRIMUS calculated Dmax to 138 Å and the Porod volume to 150387 Å³, equivalent to 94 kDa using the rule of thumb of dividing the Porod volume by 1.6 Å³/Da - a good fit of a dimer of the TgSPT1 D158 construct at 46 kDa per monomer. 15 two-fold dimer envelope models were created in DAMMIF using the ATSAS server, a consensus envelope was created by DAMAVER, and that envelope was used as a starting point for DAMMIN (58). The DAMMIN envelope was superposed with the homology model in SUPCOMB and the result was rendered in PyMol 1.7. CRYSOL (*31*) was used to calculate the theoretical X-ray scattering data from the homology model.

8

Phylogenetic analyses-The selected predicted protein sequences were aligned using CLUSTALW, edited to remove non-aligned regions, and then re-aligned in CLUSTALW with the output selected as a PHYLIP file (Supplemental 3). This alignment was then subjected to three different phylogenetic analyses: Fitch Margoliash Distance (F-MDist) (39); Randomized Axelerated Maximum Likelihood (RAxML) (40) and Phylogeny Maximum Likelihood (PhyML) (41). Bootstrap values were calculated for each analysis and used to establish the strength of the common clades in a consensus tree generated from the F-MDist data using DRAWGRAM in PHYLIP (39).

Conflict of interest: The authors declare that they have no conflicts of interest with the contents of this article.

Author contributions: JGM, JKT and AQI conducted most of the experiments and analyzed the results. LEB managed the construct assembly and analyses at OPPF. RHD optimised the protein expression. MKG performed the SAXS experimental and analyses. JAM conducted the mass spectrometry. SP cloned the cDNA. HSE constructed the conditional yeast mutant. RTS, EP and PWD designed and managed the experimental. PWD conceived the idea for the project and wrote the paper with EP and JGM.

REFERENCES

1. Chowdhury, M. N. (1986) Toxoplasmosis: a review. *J Med* **17**, 373-396
2. Dubey, J. P. (1977) Toxoplasma, Hammondia, Besnotia, Sarcocystis, and other cyst-forming coccidia of man and animals. *In: Parasitic Protozoa* **Kreier, J. P. (ed.). Academic press, New York**, 101-237
3. Coppens, I. (2013) Targeting lipid biosynthesis and salvage in apicomplexan parasites for improved chemotherapies. *Nat Rev Microbiol* **11**, 823-835
4. Coppens, I. (2014) Exploitation of auxotrophies and metabolic defects in Toxoplasma as therapeutic approaches. *Int J Parasitol* **44**, 109-120
5. Azzouz, N., Rauscher, B., Gerold, P., Cesbron-Delauw, M. F., Dubremetz, J. F., and Schwarz, R. T. (2002) Evidence for de novo sphingolipid biosynthesis in Toxoplasma gondii. *Int J Parasitol* **32**, 677-684
6. Pratt, S., Wansadhipathi-Kannangara, N. K., Bruce, C. R., Mina, J. G., Shams-Eldin, H., Casas, J., Hanada, K., Schwarz, R. T., Sonda, S., and Denny, P. W. (2013) Sphingolipid synthesis and scavenging in the intracellular apicomplexan parasite, Toxoplasma gondii. *Mol Biochem Parasitol* **187**, 43-51
7. Romano, J. D., Sonda, S., Bergbower, E., Smith, M. E., and Coppens, I. (2013) Toxoplasma gondii salvages sphingolipids from the host Golgi through the rerouting of selected Rab vesicles to the parasitophorous vacuole. *Mol Biol Cell* **24**, 1974-1995
8. Prieschl, E. E., and Baumruker, T. (2000) Sphingolipids: second messengers, mediators and raft constituents in signaling. *Immunol Today* **21**, 555-560
9. Pszenny, V., Ehrenman, K., Romano, J. D., Kennard, A., Schultz, A., Roos, D. S., Grigg, M. E., Carruthers, V. B., and Coppens, I. (2015) A Lipolytic Lecithin:Cholesterol Acyltransferase Secreted by Toxoplasma Facilitates Parasite Replication and Egress. *J Biol Chem*
10. Young, S. A., Mina, J. G., Denny, P. W., and Smith, T. K. (2012) Sphingolipid and ceramide homeostasis: potential therapeutic targets. *Biochem Res Int* **2012**, 248135
11. Simons, K., and Ikonen, E. (1997) Functional rafts in cell membranes. *Nature* **387**, 569-572
12. Lowther, J., Naismith, J. H., Dunn, T. M., and Campopiano, D. J. (2012) Structural, mechanistic and regulatory studies of serine palmitoyltransferase. *Biochem Soc Trans* **40**, 547-554
13. Hanada, K. (2003) Serine palmitoyltransferase, a key enzyme of sphingolipid metabolism. *Biochim Biophys Acta* **1632**, 16-30
14. Han, G., Gable, K., Yan, L., Natarajan, M., Krishnamurthy, J., Gupta, S. D., Borovitskaya, A., Harmon, J. M., and Dunn, T. M. (2004) The topology of the Lcb1p subunit of yeast serine palmitoyltransferase. *J Biol Chem* **279**, 53707-53716
15. Nagiec, M. M., Baltisberger, J. A., Wells, G. B., Lester, R. L., and Dickson, R. C. (1994) The LCB2 gene of Saccharomyces and the related LCB1 gene encode subunits of serine palmitoyltransferase, the initial enzyme in sphingolipid synthesis. *Proc Natl Acad Sci U S A* **91**, 7899-7902
16. Zanolari, B., Friant, S., Funato, K., Sutterlin, C., Stevenson, B. J., and Riezman, H. (2000) Sphingoid base synthesis requirement for endocytosis in Saccharomyces cerevisiae. *Embo J* **19**, 2824-2833
17. Perry, D. K. (2002) Serine palmitoyltransferase: role in apoptotic de novo ceramide synthesis and other stress responses. *Biochim Biophys Acta* **1585**, 146-152
18. Funato, K., Vallee, B., and Riezman, H. (2002) Biosynthesis and trafficking of sphingolipids in the yeast Saccharomyces cerevisiae. *Biochemistry* **41**, 15105-15114
19. Ikushiro, H., Hayashi, H., and Kagamiyama, H. (2003) Bacterial serine palmitoyltransferase: a water-soluble homodimeric prototype of the eukaryotic enzyme. *Biochim Biophys Acta* **1647**, 116-120

20. Ikushiro, H., Hayashi, H., and Kagamiyama, H. (2001) A water-soluble homodimeric serine palmitoyltransferase from Sphingomonas paucimobilis EY2395T strain. Purification, characterization, cloning, and overproduction. *J Biol Chem* **276**, 18249-18256

21. Yard, B. A., Carter, L. G., Johnson, K. A., Overton, I. M., Dorward, M., Liu, H., McMahon, S. A., Oke, M., Puech, D., Barton, G. J., Naismith, J. H., and Campopiano, D. J. (2007) The structure of serine palmitoyltransferase; gateway to sphingolipid biosynthesis. *J Mol Biol* **370**, 870-886

22. Gerold, P., and Schwarz, R. T. (2001) Biosynthesis of glycosphingolipids de-novo by the human malaria parasite Plasmodium falciparum. *Mol Biochem Parasitol* **112**, 29-37

23. Lauer, S. A., Ghori, N., and Haldar, K. (1995) Sphingolipid synthesis as a target for chemotherapy against malaria parasites. *Proc Natl Acad Sci U S A* **92**, 9181-9185

24. Haldar, K., Mohandas, N., Samuel, B. U., Harrison, T., Hiller, N. L., Akompong, T., and Cheresh, P. (2002) Protein and lipid trafficking induced in erythrocytes infected by malaria parasites. *Cell Microbiol* **4**, 383-395

25. Shams-Eldin, H., Azzouz, N., Kedees, M. H., Orlean, P., Kinoshita, T., and Schwarz, R. T. (2002) The GPI1 homologue from Plasmodium falciparum complements a Saccharomyces cerevisiae GPI1 anchoring mutant. *Mol Biochem Parasitol* **120**, 73-81

26. Denny, P. W., and Smith, D. F. (2004) Rafts and sphingolipid biosynthesis in the kinetoplastid parasitic protozoa. *Mol Microbiol* **53**, 725-733

27. Denny, P. W., Goulding, D., Ferguson, M. A., and Smith, D. F. (2004) Sphingolipid-free Leishmania are defective in membrane trafficking, differentiation and infectivity. *Mol Microbiol* **52**, 313-327

28. Ikushiro, H., Islam, M. M., Tojo, H., and Hayashi, H. (2007) Molecular characterization of membrane-associated soluble serine palmitoyltransferases from Sphingobacterium multivorum and Bdellovibrio stolpii. *J Bacteriol* **189**, 5749-5761

29. Berrow, N. S., Alderton, D., Sainsbury, S., Nettleship, J., Assenberg, R., Rahman, N., Stuart, D. I., and Owens, R. J. (2007) A versatile ligation-independent cloning method suitable for high-throughput expression screening applications. *Nucleic Acids Res* **35**, e45

30. Bird, L. E. (2011) High throughput construction and small scale expression screening of multi-tag vectors in Escherichia coli. *Methods* **55**, 29-37

31. Svergun, D., Barberato, C., and Koch, M. H. J. (1995) CRYSOL – a program to evaluate X-ray solution scattering of biological macromolecules from atomic coordinates. *J. Appl. Crystallogr.* **28**, 768-773

32. Zuegge, J., Ralph, S., Schmuker, M., McFadden, G. I., and Schneider, G. (2001) Deciphering apicoplast targeting signals--feature extraction from nuclear-encoded precursors of Plasmodium falciparum apicoplast proteins. *Gene* **280**, 19-26

33. van Dooren, G. G., and Striepen, B. (2013) The Algal Past and Parasite Present of the Apicoplast. *Annu Rev Microbiol*

34. Agrawal, S., van Dooren, G. G., Beatty, W. L., and Striepen, B. (2009) Genetic evidence that an endosymbiont-derived endoplasmic reticulum-associated protein degradation (ERAD) system functions in import of apicoplast proteins. *J Biol Chem* **284**, 33683-33691

35. Ramakrishnan, S., Docampo, M. D., Macrae, J. I., Pujol, F. M., Brooks, C. F., van Dooren, G. G., Hiltunen, J. K., Kastaniotis, A. J., McConville, M. J., and Striepen, B. (2012) Apicoplast and endoplasmic reticulum cooperate in fatty acid biosynthesis in apicomplexan parasite Toxoplasma gondii. *J Biol Chem* **287**, 4957-4971

36. Zeitvogel, F., and Obst, M. (2016) ScatterJn: An ImageJ Plugin for Scatterplot-Matrix Analysis and Classification of Spatially Resolved Analytical Microscopy Data. *Journal of Open Research Software* **4**

37. Zeitvogel, F., Schmid, G., Hao, L., Ingino, P., and Obst, M. (2016) ScatterJ: An ImageJ plugin for the evaluation of analytical microscopy datasets. *J Microsc* **261**, 148-156

38.   Larkin, M. A., Blackshields, G., Brown, N. P., Chenna, R., McGettigan, P. A., McWilliam, H., Valentin, F., Wallace, I. M., Wilm, A., Lopez, R., Thompson, J. D., Gibson, T. J., and Higgins, D. G. (2007) Clustal W and Clustal X version 2.0. *Bioinformatics* **23**, 2947-2948

39.   Felsenstein, J. (1989) Mathematics vs. Evolution: Mathematical Evolutionary Theory. *Science* **246**, 941-942

40.   Stamatakis, A. (2014) RAxML version 8: a tool for phylogenetic analysis and post-analysis of large phylogenies. *Bioinformatics* **30**, 1312-1313

41.   Guindon, S., and Gascuel, O. (2003) A simple, fast, and accurate algorithm to estimate large phylogenies by maximum likelihood. *Syst Biol* **52**, 696-704

42.   Arisue, N., and Hashimoto, T. (2015) Phylogeny and evolution of apicoplasts and apicomplexan parasites. *Parasitol Int* **64**, 254-259

43.   Huitema, K., Van Den Dikkenberg, J., Brouwers, J. F., and Holthuis, J. C. (2004) Identification of a family of animal sphingomyelin synthases. *Embo J* **23**, 33-44

44.   Di Tommaso, P., Moretti, S., Xenarios, I., Orobitg, M., Montanyola, A., Chang, J. M., Taly, J. F., and Notredame, C. (2011) T-Coffee: a web server for the multiple sequence alignment of protein and RNA sequences using structural information and homology extension. *Nucleic Acids Res* **39**, W13-17

45.   Denny, P. W., Preiser, P. R., Williamson, D. H., and Wilson, R. J. M. (1998) Evidence for a single origin of the 35 kbp plastid DNA in apicomplexans. *Protist*, 51-59

46.   Denny, P. W., Shams-Eldin, H., Price, H. P., Smith, D. F., and Schwarz, R. T. (2006) The protozoan inositol phosphorylceramide synthase: a novel drug target that defines a new class of sphingolipid synthase. *J Biol Chem* **281**, 28200-28209

47.   Herm-Gotz, A., Weiss, S., Stratmann, R., Fujita-Becker, S., Ruff, C., Meyhofer, E., Soldati, T., Manstein, D. J., Geeves, M. A., and Soldati, D. (2002) Toxoplasma gondii myosin A and its light chain: a fast, single-headed, plus-end-directed motor. *Embo J* **21**, 2149-2158

48.   Hager, K. M., Striepen, B., Tilney, L. G., and Roos, D. S. (1999) The nuclear envelope serves as an intermediary between the ER and Golgi complex in the intracellular parasite Toxoplasma gondii. *J Cell Sci* **112 (Pt 16)**, 2631-2638

49.   Schneider, C. A., Rasband, W. S., and Eliceiri, K. W. (2012) NIH Image to ImageJ: 25 years of image analysis. *Nat Meth* **9**, 671-675

50.   Pfluger, S. L., Goodson, H. V., Moran, J. M., Ruggiero, C. J., Ye, X., Emmons, K. M., and Hager, K. M. (2005) Receptor for retrograde transport in the apicomplexan parasite Toxoplasma gondii. *Eukaryot Cell* **4**, 432-442

51.   Soding, J., Biegert, A., and Lupas, A. N. (2005) The HHpred interactive server for protein homology detection and structure prediction. *Nucleic Acids Res* **33**, W244-248

52.   Ikushiro, H., Islam, M. M., Okamoto, A., Hoseki, J., Murakawa, T., Fujii, S., Miyahara, I., and Hayashi, H. (2009) Structural insights into the enzymatic mechanism of serine palmitoyltransferase from Sphingobacterium multivorum. *J Biochem* **146**, 549-562

53.   Eswar, N., Webb, B., Marti-Renom, M. A., Madhusudhan, M. S., Eramian, D., Shen, M. Y., Pieper, U., and Sali, A. (2006) Comparative protein structure modeling using Modeller. *Curr Protoc Bioinformatics* **Chapter 5**, Unit 5 6

54.   Fiser, A., and Sali, A. (2003) ModLoop: automated modeling of loops in protein structures. *Bioinformatics* **19**, 2500-2501

55.   De Maria Antolinos, A., Pernot, P., Brennich, M. E., Kieffer, J., Bowler, M. W., Delageniere, S., Ohlsson, S., Malbet Monaco, S., Ashton, A., Franke, D., Svergun, D., McSweeney, S., Gordon, E., and Round, A. (2015) ISPyB for BioSAXS, the gateway to user autonomy in solution scattering experiments. *Acta Crystallogr D Biol Crystallogr* **71**, 76-85

56.   Basham, M., Filik, J., Wharmby, M. T., Chang, P. C., El Kassaby, B., Gerring, M., Aishima, J., Levik, K., Pulford, B. C., Sikharulidze, I., Sneddon, D., Webber, M., Dhesi, S. S., Maccherozzi, F., Svensson, O., Brockhauser, S., Naray, G., and Ashton, A. W. (2015) Data Analysis WorkbeNch (DAWN). *J Synchrotron Radiat* **22**, 853-858

57. Petoukhov, M. V., Franke, D., Shkumatov, A. V., Tria, G., Kikhney, A. G., Gajda, M., Gorba, C., Mertens, H. D., Konarev, P. V., and Svergun, D. I. (2012) New developments in the program package for small-angle scattering data analysis. *J Appl Crystallogr* **45**, 342-350

58. Tuukkanen, A. T., Kleywegt, G. J., and Svergun, D. I. (2016) Resolution of ab initio shapes determined from small-angle scattering. *IUCrJ* **3**, 440-447

59. Gouet, P., Robert, X., and Courcelle, E. (2003) ESPript/ENDscript: Extracting and rendering sequence and 3D information from atomic structures of proteins. *Nucleic Acids Res* **31**, 3320-3323

FOOTNOTES

The abbreviations used are: SPT, serine palmitoyltransferase; KDS, 3-ketodihydrosphingosine; PLP, pyridoxal phosphate; ER, endoplasmic reticulum; LCB, long chain base; SM, sphingomyelin; GSL, glycosphingolipid; IPC, inositol phosphorylceramide, SAXS, small-angle X-ray scattering.

FIGURE LEGENDS

FIGURE 1. Schematic showing the chemical reaction catalysed by the serine palmitoyltransferase (SPT) in which the enzyme catalyses the condensation of serine and palmitoyl-CoA to form 3-ketodihydrosphinganine (KDS) with the release of Coenzyme A (HSCoA) and CO_2.

FIGURE 2. Sequence alignment of the predicted serine palmitoyltransferase (SPT) from 4 members of the Apicomplexa (*Toxoplasma gondii* – TgSPT1 and 2; *Eimeria tenella* – EtSPT; *Plasmodium falciparum* – PfSPT; and *P. vivax* – PvSPT) and the characterised enzyme from the prokaryote *Sphingomonas paucimobilis* (SpSPT)*. Conserved residues (including those in the active site) identified by analyses of the SpSPT structure and homology modelling of the human functional orthologue (LCB2), are highlighted in red, with red text denoting similarity. Blue boxes denote conserved domains. The canonical lysine demonstrated to form an internal aldimine with the co-factor PLP at SpSPT position 265 is highlighted (*21*). The *N*-terminal extensions unique to the predicted apicomplexan enzymes harbour a transmembrane domain predicted by TMPRED (TMD, bold underlined). The figure was produced using ESPript 3.0 (59).

FIGURE 3. Transformed auxotrophic yeast grown on selective media with either galactose (*A*) or glucose (*B*). Both ScLcb2 and TgSPT1 rescue the mutant *S. cerevisiae* which are deficient in endogenous ScLcb2 when grown in the presence of glucose (*B*). pRS246 is the empty vector control.

FIGURE 4. Mass spectrometry positive ion spectrum of lipids extracted from *in vitro* reaction of TgSPT1 Δ158 with serine and palmitoyl CoA as substrates. The peak 300.29 corresponds to the mass of 3-ketodihydrosphinganine.

FIGURE 5. *A* SAXS generated envelope overlaying a homology model of the TgSPT1 dimer. *B* Small-angle X-ray scattering data (binned mode as blue dots), superimposed with the calculated scattering curve using the homology mode (in red). **C** Close-up of the PLP binding site of the homology model of TgSPT1 based on the crystal structure of SPT from *S. multivorum*. The key PLP binding residues depicted with cyan bonds in a ball-and-stick representation are conserved in the family (see Figure 2). The numbering corresponds to the TgSPT1 sequence. Note that Ser429/B belongs to the second subunit of the homodimer.

FIGURE 6. *Toxoplasma* stained for ectopically expressed TgSPT1-TY (*A* - AlexaFluor594, red) and endogenous TgSPT1 (*E* - AlexaFluor594, red); ectopically expressed ER marker GFP-HDEL (*B* and *F* - AlexaFluor488, green); and DNA (*C* and *G* - DAPI, blue). Co-localisation of TgSPT1, ectopically expressed and endogenous, with GFP-HDEL is shown in merge of *A* and *B* (*D* - yellow) and *E* and *F* (*H* - yellow) repsectively. Scale bar is equivalent to 10 μm.

FIGURE 7. Endogenous TgSPT1 (*A* - AlexaFluor594, red) and ectopically expressed ER marker GFP-HDEL (*B* - AlexaFluor488, green) co-localise as shown in the merged image (*D* - yellow). Scale bar is

equivalent to 10 μm. In support of this, the scatterplot (*E*) demonstrates the strong correlation of TgSPT1 (antiSPT-AF594) with GFP-HDEL (antiGFP-AF488). In contrast, neither TgSPT1 (antiSPT-AF594) nor GFP-HDEL (antiGFP-AF488) show any significant correlation with DAPI-stained (*C*) nuclei (*F* and *G*). The colour scale represents the number of pixels as indicated.

FIGURE 8. *A* Schematic illustrating the gene arrangement in the region surrounding the encoded *Cryptosporidum muris* serine palmitoyltransferase, compared with the syntenic regions of *C. parum* and *C. hominis* chromosome 6. *B* Phylogenetic tree produced from a genetic distance matrix showing the relationship between the eukaryotic catalytic subunit of serine palmitoyltransferase (LCB2) and the prokaryotic and apicomplexan orthologues (SPT). The Opistokonta (animals and fungi) are coloured blue; the Excavata (subgroup of unicellular eukaryotes) are yellow; Amoebozoa (amoeboid protozoa) are grey; Archaeplastida (plants and algae, containing cyanobacterium-derived plastid) are green; Rodophyta (a subgroup of the Archaeplastida - red algae) are red; Chromalveolata (unicellular eukaryotes containing red algal derived plastid) are turquoise; Sphingomonadales (alphaproteobacteria with the ability to synthesize sphingolipids) are pink. The bootstrap values of the major clades are shown where they are greater than 60 at common nodes for the three methodologies employed – Fitch Margoliash Distance (F-MDist); Randomized Axelerated Maximum Likelihood (RAxML); and Phylogeny Maximum Likelihood (PhyML). The non-catalytic subunit of the human serine palmitoyltransferase (HsLCB1) was utilised as the outgroup. Sequences used in the analyses were equivalent to those aligned to TgSPT1 amino acid 228 to 411.

Sequence information:

LCB1 - serine palmitoyltransferase subunit 1; LCB2 - palmitoyltransferase subunit 2; SPT - serine palmitoyltransferase

NBCI accession numbers:

HsLCB1: *Homo sapiens* - EAW62806; HsLCB2: *Homo sapiens* sphingomyelin synthase subunit 2 - NP_004854; MmLCB2: *Mus muscalis* - NP_035609; DmLCB2: *Drosophila melanogaster* - BAA83721; CeLCB2: *Caenorhabditis elegans* - Q20375; DrLCB2 – *Danio rerio* - NP_001108213; OsLCB2: *Oryza sativa* - BAD88168.1; AtLCB2: *Arabidopsis thaliana* - NP_001031932.1; DdLCB2: *Dictyostelium discodium* - XP_635115

Joint Genome Institute accession numbers: NvLCB2: *Nematostella vectensis* – 241814; MbLCB2: *Monosiga brevicollis* – 34401; PtLCB2: *Populus trichocarpa* – 834365; OtLCB2: *Ostreococcus tauri* – 16411; TpLCB2: *Thalassiosira pseudonana* – 255691; PrLCB2: *Phytophthora ramorum* – 71166; NgLCB2: *Naegleria gruberi* – 82916; SpSPT: *Sphingomonas paucimobilis* - Q93UV0_PSEPA; SmSPT: *Sphingobacterium multivorum* - A7BFV6_9SPHI; SsSPT: *Sphingobacterium spiritivorum* - A7BFV7_9SPHI; BsSPT: *Bacteriovorax stolpii* - A7BFV8_9DELT

Universal Protein Resource accession numbers: ScLCB2: *Saccharomyces cerevisiae* - P40970; CnLCB2: *Cryptococcus neoformans* - J9VYF7; SpLCB2: *Schizosaccharomyces pombe* - Q09925; AnLCB2: *Aspergillus nidulans* - Q5BEC8; RoLCB2: *Rhizopus oryzae* - I1BXF5

Cyanidioschyzon merolae Genome Project accession numbers: CmLCB2: *Cyanidioschyzon merolae* - CMJ240C

ToxoDB accession numbers: TgSPT1: *Toxoplasma gondii* - TGME49_090980; TgSPT2 - TGME49_090970

GeneDB accession numbers: PfSPT: *Plasmodium falciparum* - PF14_0155; PvSPT – *P. vivax;* CmSPT: *Cryptosporidium muris* - B6ACS8_CRYMR; TbLCB2: *Trypanosoma brucei* - Tb927.10.4050; LmLCB2: *Leishmania major* - LmjF35.0320

Sanger Institute accession numbers: EtSPT: *Eimeria tenella* - dev_EIMER_contig_00020813
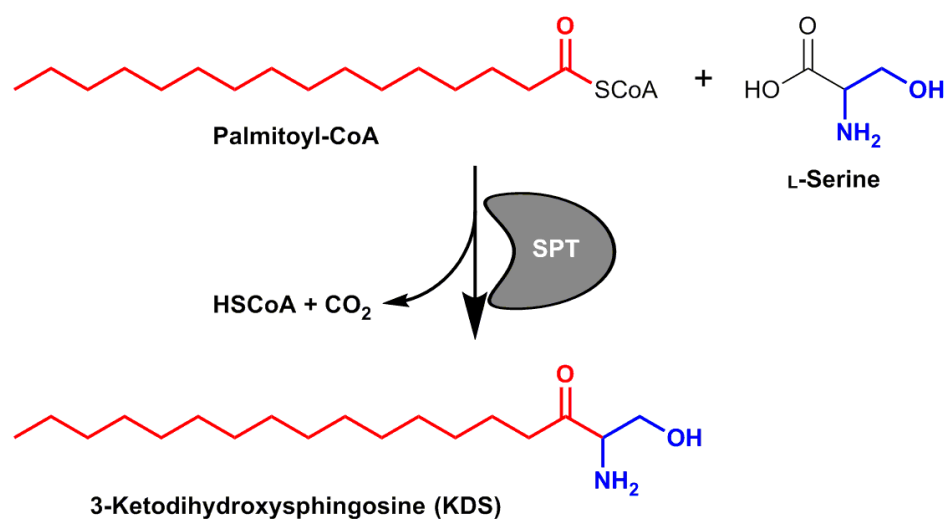
FIGURE 1

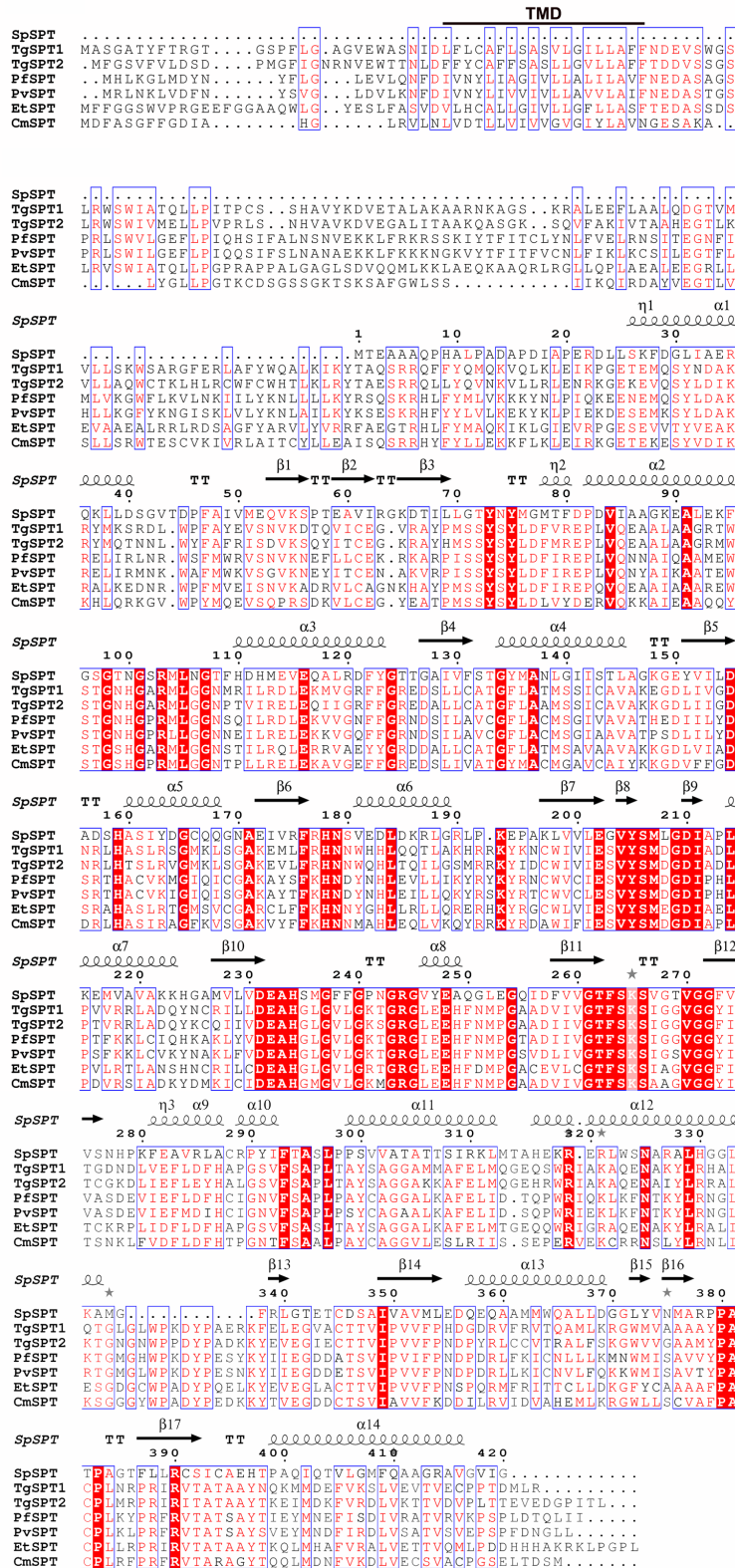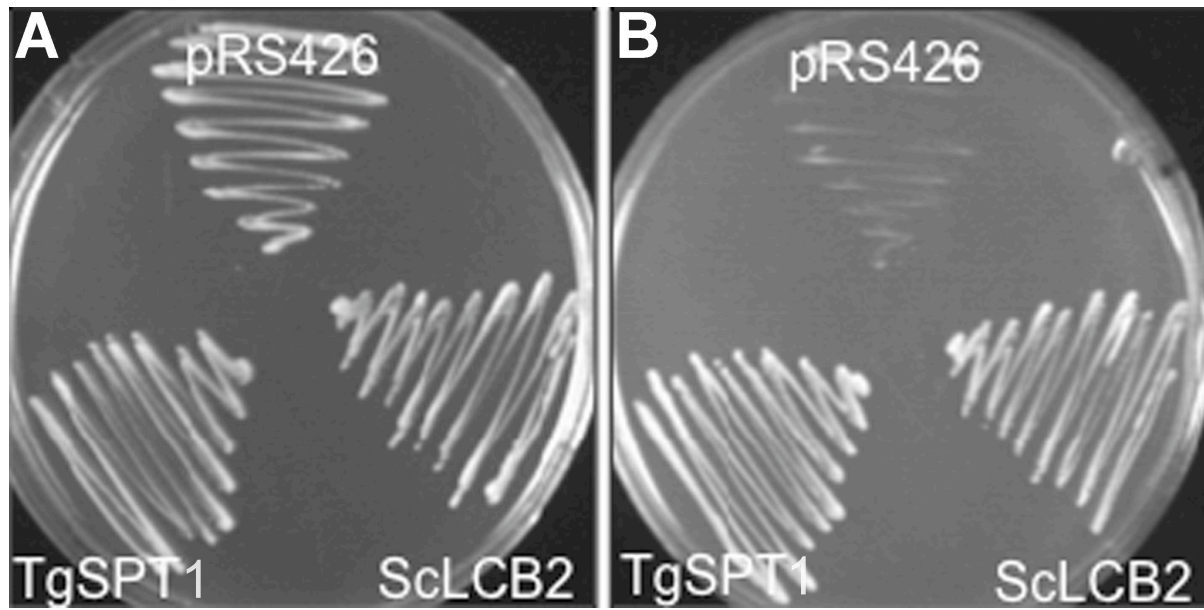**Palmitoyl-CoA**

L-Serine

SPT

$HSCoA + CO_2$

3-Ketodihydroxysphingosine (KDS)

FIGURE 2

FIGURE 3

FIGURE 4

C₁₈H₃₇NO₂, Exact Mass: 299.2824,
m/z: calc. 300.2858 [M+H]⁺, found 300.2907 [M+H]⁺
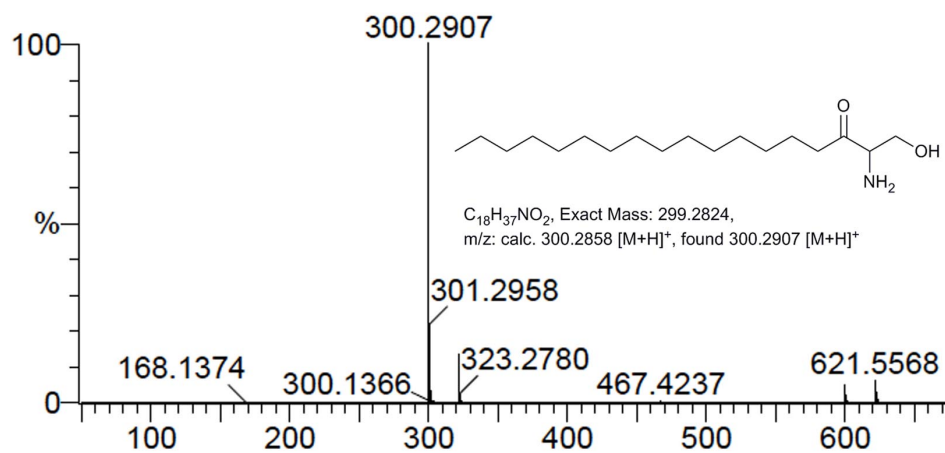
FIGURE 5

A
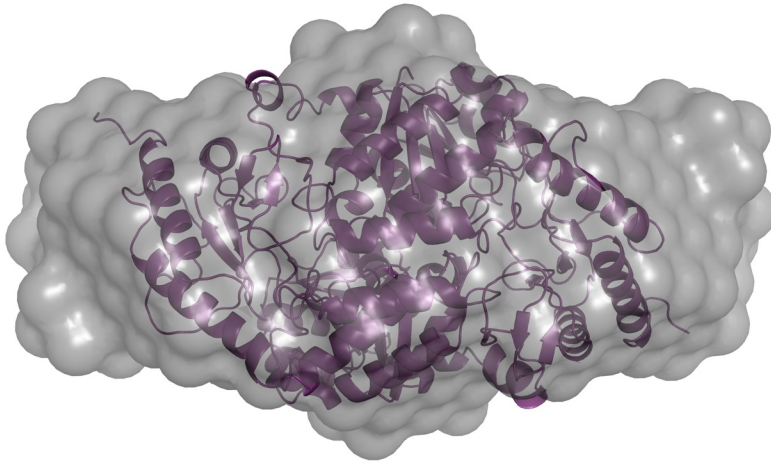
B
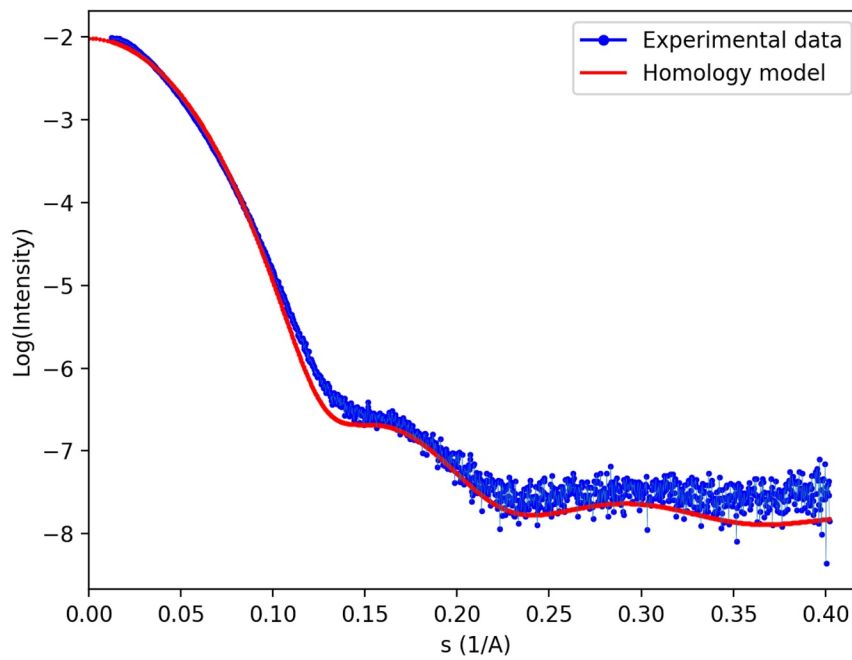
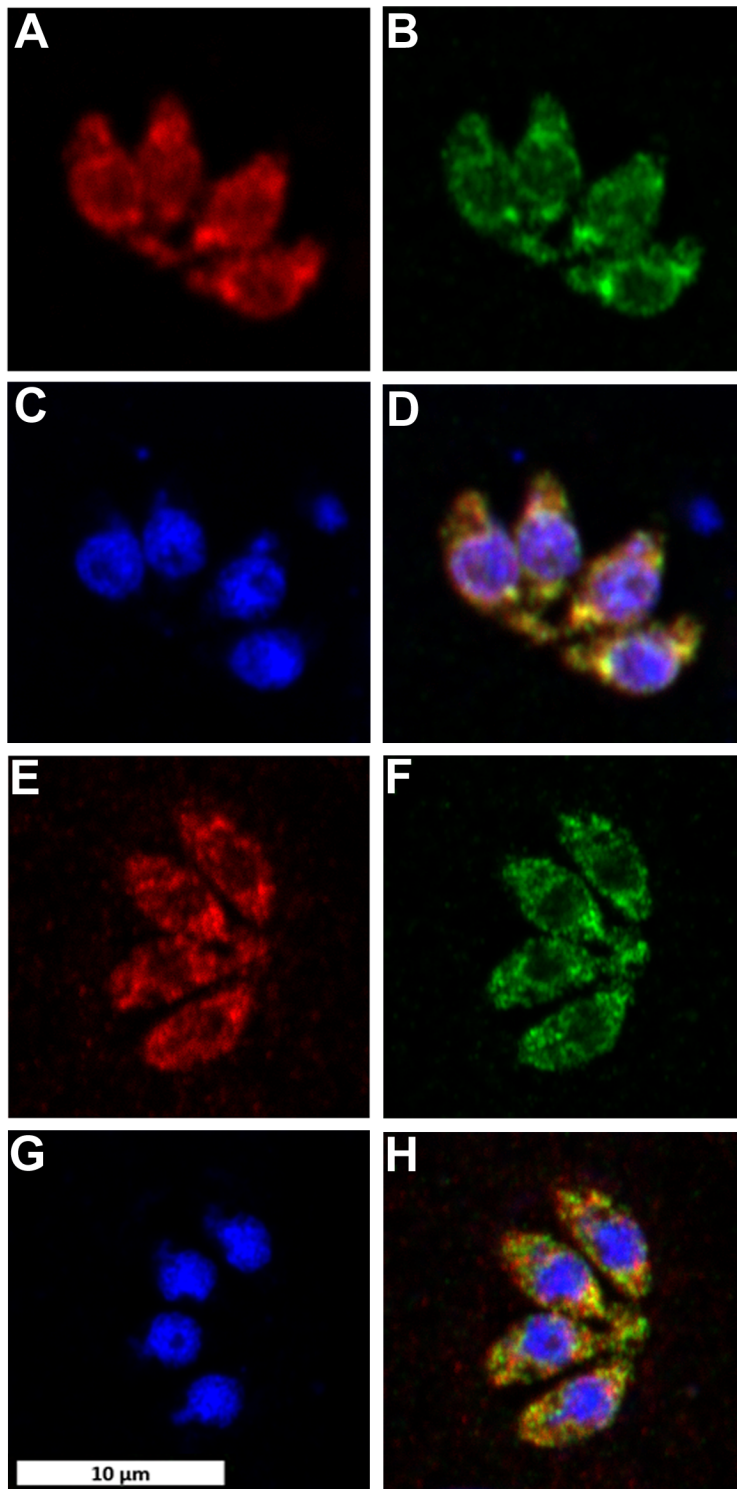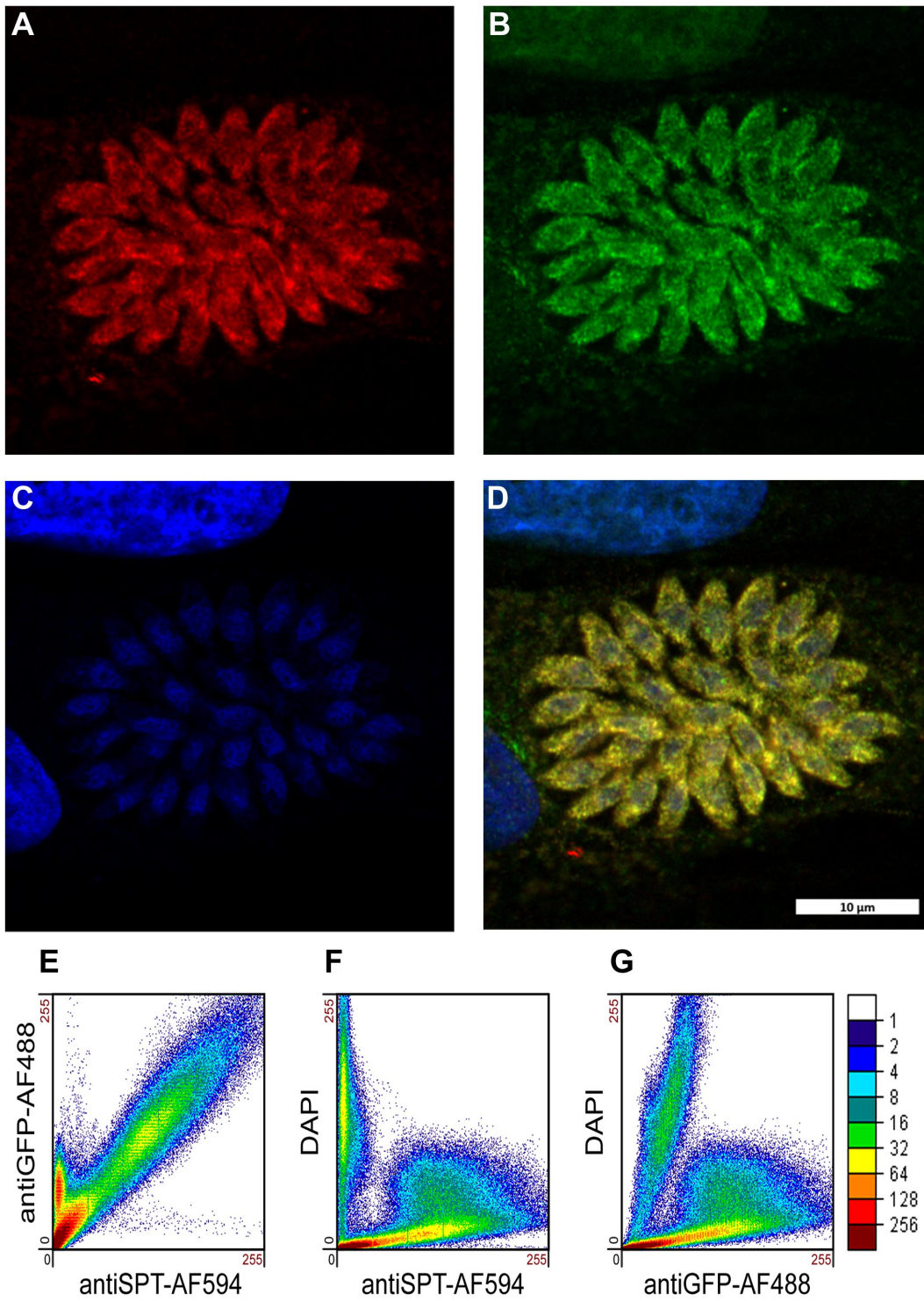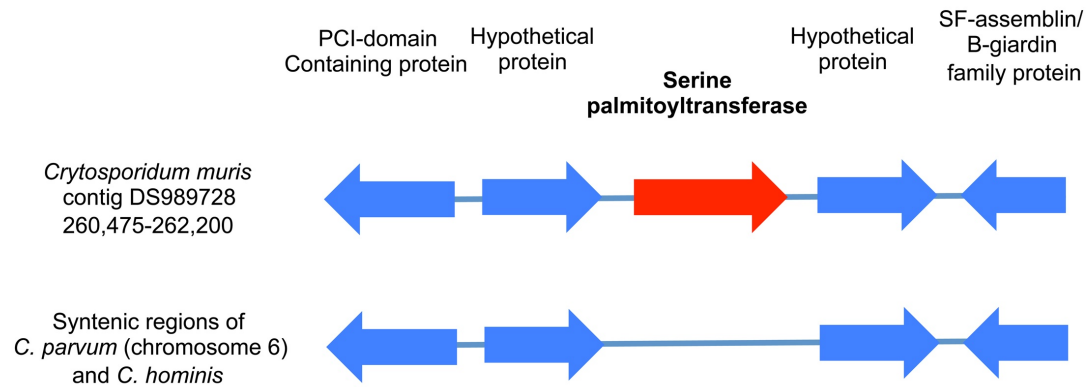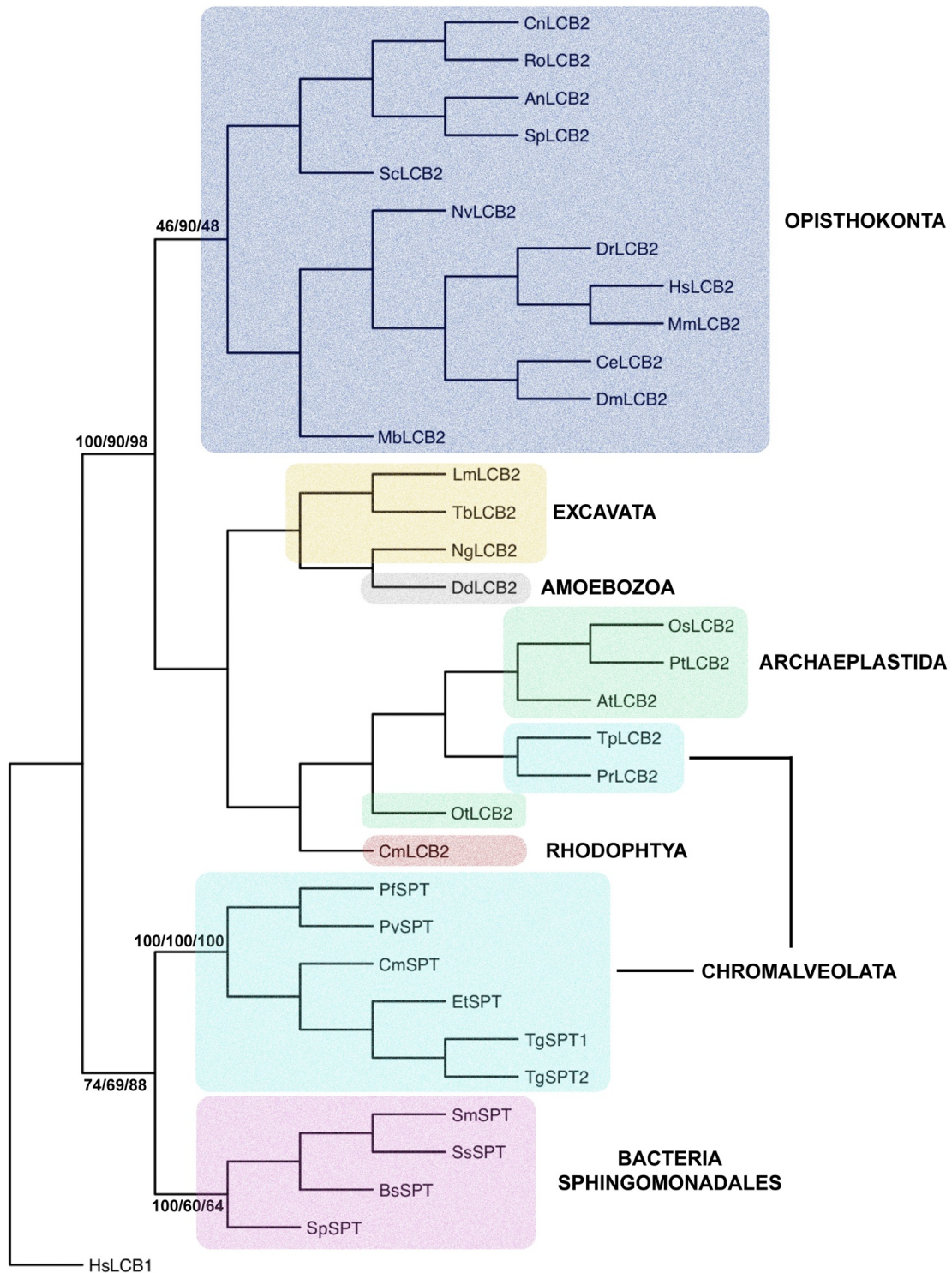**C**
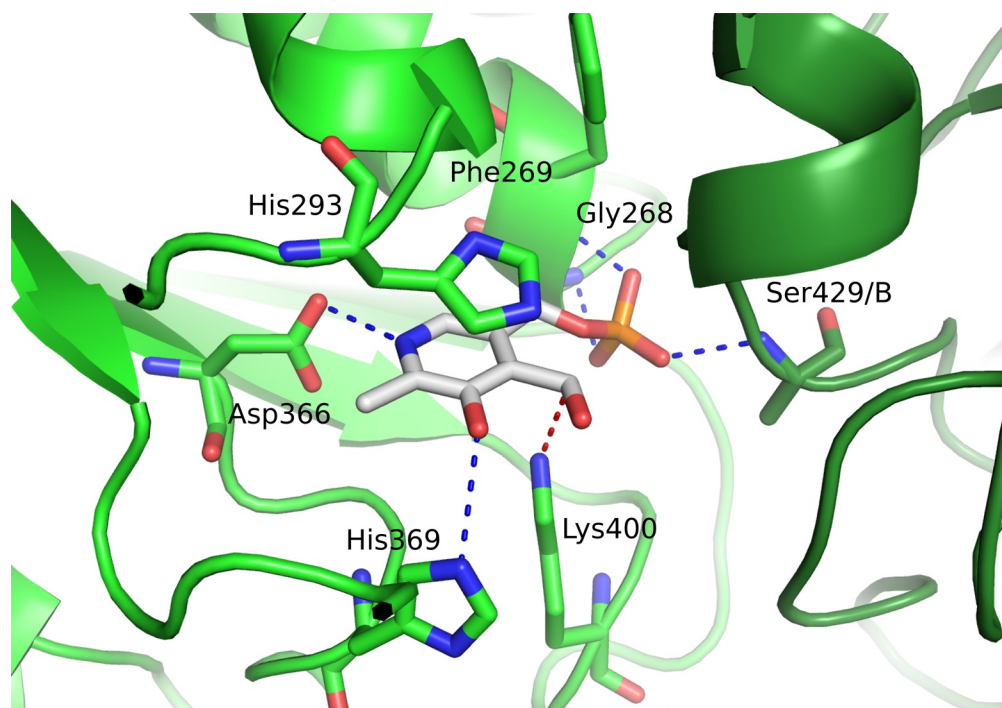
FIGURE 6

FIGURE 7

FIGURE 8

A

B

Functional and phylogenetic evidence of a bacterial origin for the first enzyme in sphingolipid biosynthesis in a phylum of eukaryotic protozoan parasites

John G. Mina, Julie K. Thye, Amjed Q.I. Alqaisi, Louise E. Bird, Robert H. Dods, Morten K. Groftehauge, Jackie A. Mosely, Steven Pratt, Hosam Shams-Eldin, Ralph T. Schwarz, Ehmke Pohl and Paul W. Denny

Access the most updated version of this article at doi: 10.1074/jbc.M117.792374

Alerts:
- When this article is cited
- When a correction for this article is posted

Click here to choose from all of JBC's e-mail alerts

Supplemental material:
http://www.jbc.org/content/suppl/2017/06/02/M117.792374.DC1

This article cites 0 references, 0 of which can be accessed free at
http://www.jbc.org/content/early/2017/06/02/jbc.M117.792374.full.html#ref-list-1